

Temporal relaxation of gapped many-body quantum systems

Peter Reimann¹, Ben N. Balz¹, Jonas Richter², and Robin Steinigeweg²

¹*Fakultät für Physik, Universität Bielefeld, 33615 Bielefeld, Germany*

²*Department of Physics, University of Osnabrück, 49069 Osnabrück, Germany*

Typicality of the orthogonal dynamics (TOD) is established as a generic feature of temporal relaxation processes in isolated many-body quantum systems. The basic idea in the simplest case is that the transient non-equilibrium behavior is mainly governed by the component of the time-evolved system state parallel to the initial state, while the orthogonal component appears as equilibrated right from the beginning. The main emphasis is laid on the largely unexplored and particularly challenging case that one energy level exhibits a much larger population than all the others. Important examples are gapped many-body systems at low energies, for instance due to a quantum quench. A general analytical prediction is derived and is found to compare very well with various numerically exact results.

I. INTRODUCTION

Equilibration and thermalization of possibly far-from-equilibrium initial states in isolated many-body quantum systems have recently attracted a considerable amount of theoretical and experimental interest [1–6]. In particular, despite the well-known quantum revival and reversibility properties of the system’s unitary time evolution [7], it could be shown [8–13] that rather weak assumptions are sufficient to guarantee equilibration in the following sense: The expectation values of a given observable stay extremely close to a constant value for the vast majority of all sufficiently late times, i.e., after the initial transients have died out. As detailed in [8–13], to demonstrate equilibration in this sense it is sufficient that the system’s energy spectrum does not exhibit some highly non-generic features, and that every single of the extremely numerous energy levels is only weakly populated by the initial state. Somewhat less appreciated so far is the fact that the latter condition is actually not an indispensable prerequisite: Namely, equilibration is still guaranteed if there is one exceptional, non-small energy level population [12, 13]. In particular, the requirement from [9–11] that the so-called effective dimension or inverse participation ration (IPR) must be large, is then no longer fulfilled.

The main goal of our present work is to gain analytical insight into the detailed temporal decay of the above mentioned initial transients, especially (but not exclusively) in cases with a non-small population of one level. The first reason is that their temporal relaxation behavior turns out to be particularly non-trivial to predict. Second, they have been hardly considered before, yet seem of considerable conceptual and practical interest.

Typical examples where such a scenario may naturally arise are systems with an energy gap between the ground state and the excited states. Starting in the ground state (or some more general low energy state) and then suddenly changing a system parameter (quantum quench) may often result in a far-from-equilibrium initial state with a large population of the “new” (post-quench) ground state and a small population of all other states

[14]. For instance, such gaps commonly arise in solid-state insulators as a consequence of their electronic band structure. Moreover, other possibilities than quenches to generate initial states with one non-small level population are easily conceivable.

Further examples to which our present theory should be readily applicable are systems which, instead of a gap, exhibit a highly degenerate ground state, such as sawtooth Heisenberg chains, or kagomé, checkerboard, and pyrochlore spin lattices, see [15] and references therein. Finally, also more conventional situations without any non-small populations, gaps, or high degeneracies will be included as special cases.

II. GENERAL FRAMEWORK

We consider an isolated many-body quantum system, modeled by a Hamiltonian H with eigenvalues E_n and eigenvectors $|n\rangle$. A given initial state $|\psi_0\rangle$ with components $c_n := \langle n|\psi_0\rangle$ then evolves in time as ($\hbar = 1$)

$$|\psi_t\rangle = e^{-iHt}|\psi_0\rangle = \sum_{n=0}^N c_n e^{-iE_n t} |n\rangle, \quad (1)$$

where, depending on the specific model under consideration, N may be large but finite or infinite. Further, $p_n := |c_n|^2$ are the level populations with $\sum_{n=0}^N p_n = 1$.

In case that, say, E_n is degenerate, we choose $|n\rangle$ as the (normalized) projection of $|\psi_0\rangle$ onto the corresponding eigenspace \mathcal{H}_n . Hence, all other basis vectors of \mathcal{H}_n play no role and can be omitted in (1). In other words, while the actual system may well exhibit degeneracies, we can and will exclude them in (1).

Choosing $n = 0$ for the specific level with a possibly non-small population p_0 , and ignoring the trivial case $p_0 = 1$, we rewrite (1) as

$$|\psi_t\rangle = c_0 e^{-iE_0 t} |0\rangle + \sqrt{1-p_0} |\psi'_t\rangle \quad (2)$$

$$|\psi'_t\rangle := \sum_{n=1}^N c'_n e^{-iE_n t} |n\rangle, \quad c'_n := \frac{c_n}{\sqrt{1-p_0}}. \quad (3)$$

It follows that $|\psi'_t\rangle$ and $|0\rangle$ are orthonormalized. Defining

$$\alpha'_t := \langle \psi'_0 | \psi'_t \rangle, \quad P := \mathbb{1} - |\psi'_0\rangle\langle \psi'_0|, \quad (4)$$

$$|\psi_t^\perp\rangle := P|\psi'_t\rangle/\beta'_t, \quad \beta'_t := \langle \psi'_t | P|\psi'_t \rangle^{1/2}, \quad (5)$$

one readily concludes [16] that $|\psi_t\rangle = \alpha'_t|\psi'_0\rangle + \beta'_t|\psi_t^\perp\rangle$ and thus

$$|\psi_t\rangle = c_0 e^{-iE_0 t} |0\rangle + \alpha_t |\psi'_0\rangle + \beta_t |\psi_t^\perp\rangle, \quad (6)$$

$$\alpha_t := \alpha'_t \sqrt{1-p_0}, \quad \beta_t := \beta'_t \sqrt{1-p_0}. \quad (7)$$

Furthermore, $|0\rangle$, $|\psi'_0\rangle$, and $|\psi_t^\perp\rangle$ are normalized and pairwise orthogonal, implying $\langle \psi_t^\perp | \psi_0 \rangle = 0$ and

$$\beta_t = \sqrt{1-p_0 - |\alpha_t|^2}. \quad (8)$$

The main virtue of (6), which will be heavily exploited in the following, is that the system dynamics has been decomposed into three orthogonal components, two of them pointing into the ‘‘special directions’’ $|0\rangle$ and $|\psi'_0\rangle$ (and encapsulating the initial state $|\psi_0\rangle$), and an ‘‘orthogonal rest’’ $|\psi_t^\perp\rangle$.

III. ANALYTICAL PREDICTION

Given an observable (Hermitian operator) A , we can infer from (6) and (8) that

$$\begin{aligned} \mathcal{A}_t &:= \langle \psi_t | A | \psi_t \rangle = p_0 \langle 0 | A | 0 \rangle + |\alpha_t|^2 \langle \psi'_0 | A | \psi'_0 \rangle \\ &\quad + \beta_t^2 \langle \psi_t^\perp | A | \psi_t^\perp \rangle + q_t + q_t^*, \end{aligned} \quad (9)$$

$$q_t := c_0^* e^{iE_0 t} (\alpha_t \langle 0 | A | \psi'_0 \rangle + r_t) + \alpha_t^* s_t, \quad (10)$$

$$r_t := \beta_t \langle 0 | A | \psi_t^\perp \rangle, \quad s_t := \beta_t \langle \psi'_0 | A | \psi_t^\perp \rangle. \quad (11)$$

Exploiting (5) and (7), we rewrite r_t from (11) as $\langle v | \psi_t^\perp \rangle$, where $|v\rangle := \sqrt{1-p_0} P A |0\rangle$. With (3) we thus obtain

$$r_t = \sum_{n=1}^N b_n e^{-iE_n t}, \quad b_n := c'_n \langle v | n \rangle. \quad (12)$$

Indicating time averages over all $t \geq 0$ by an overbar, i.e., $\overline{\bullet} := \lim_{T \rightarrow \infty} \int_0^T \bullet dt / T$, and recalling that degeneracies are excluded in (1), it follows that

$$\overline{|r_t|^2} = \sum_{n=1}^N |b_n|^2 = \sum_{n=1}^N |c'_n|^2 \langle v | n \rangle \langle n | v \rangle. \quad (13)$$

Hence, $\overline{|r_t|^2}$ can be upper bounded by $\langle v | v \rangle \max_{n \geq 1} |c'_n|^2$, and with (3) by κp_{\max} , where $\kappa := \langle 0 | A P A | 0 \rangle$ and $p_{\max} := \max_{n \geq 1} p_n$. Denoting by $\|\cdot\|$ the operator norm, and exploiting that $\|P\| = 1$ since P from (4) is a projector, it follows that $\kappa \leq \|A P A\| \leq \|A\|^2$, and thus $\overline{|r_t|^2} \leq \|A\|^2 p_{\max}$. Considering $|r_t|$ as a random variable with uniformly distributed $t \geq 0$, we can invoke Markov’s inequality to conclude

$$\text{Prob}(|r_t| \leq \|A\| p_{\max}^{1/3}) \geq 1 - p_{\max}^{1/3}, \quad (14)$$

where the left hand side denotes the probability that $|r_t| \leq \|A\| p_{\max}^{1/3}$ for a randomly drawn $t \in [0, \infty)$. It is plausible, and has been worked out in detail e.g. in [12], that essentially the same conclusion remains true for a randomly drawn $t \in [0, T]$, provided T is sufficiently large. Assuming

$$p_{\max} := \max_{n \geq 1} p_n \ll 1, \quad (15)$$

it follows that the contribution of r_t to (10) is negligible (compared to the full range of possible values, which \mathcal{A}_t in (9) in principle could take) for the vast majority of all sufficiently large t , symbolically indicated as $r_t \simeq 0$. The assumption (15) means that all energy levels with the possible exception of $|0\rangle$ must be weakly populated, and represents, as said in the introduction, the key prerequisite of our present approach.

Likewise, (15) implies for the vast majority of all sufficiently large t that $s_t \simeq 0$, $\alpha_t \simeq 0$, and $\mathcal{A}_t \simeq \overline{\mathcal{A}} := \overline{\mathcal{A}_t}$. The latter relation is tantamount to the equilibration results mentioned at the beginning of the paper, see also Refs. [12, 13] for its detailed derivation. By exploiting (11) and $\alpha_t \simeq 0$ in (8), we furthermore obtain

$$\langle u | \psi_t^\perp \rangle \simeq 0, \quad \langle w | \psi_t^\perp \rangle \simeq 0, \quad (16)$$

where $|u\rangle := \sqrt{1-p_0} A |0\rangle$ and $|w\rangle := \sqrt{1-p_0} A |\psi'_0\rangle$. Introducing all these findings into (9) implies

$$\langle \psi_t^\perp | A | \psi_t^\perp \rangle \simeq \frac{\overline{\mathcal{A}} - p_0 \langle 0 | A | 0 \rangle}{1 - p_0}. \quad (17)$$

Notably, the special case that *all* level populations p_n are small is still admitted by our approach, and is – in view of (15) – most conveniently recovered by considering $|0\rangle$ as a purely formal ‘‘ancillary level’’ with $p_0 = 0$ and hence $c_0 = 0$ in (1). Moreover, all primed quantities in (2)-(7) then coincide with their unprimed counterparts.

So far, the approximations (16)-(17) only pertain to the vast majority of all sufficiently late times (see below (15)). Our next goal is to also cover the earlier times.

For simplicity, we first focus again on the special case $c_0 = 0$ from above. The time-evolved state $|\psi_t\rangle$ is thus decomposed according to (6) into two orthonormalized components $|\psi'_0\rangle$ and $|\psi_t^\perp\rangle$, the first being identical and the second orthogonal to the initial state $|\psi_0\rangle$ (see above (8)). The main difference of the earlier times t compared to the later ones is that $|\psi_t\rangle$ still somehow ‘‘remembers’’ the specific non-equilibrium properties of $|\psi_0\rangle$. But since $|\psi_t^\perp\rangle$ is always orthogonal to $|\psi_0\rangle$, it seems reasonable to expect that this remembrance of the initial state $|\psi_0\rangle$ will mainly concern the component of $|\psi_t\rangle$ parallel to $|\psi_0\rangle$, while the (normalized) contribution $|\psi_t^\perp\rangle$ orthogonal to $|\psi_0\rangle$ will behave similarly at early and at later times with respect to some very basic properties, such as the scalar product with a fixed vector appearing in (16), or the expectation value on the left hand side of (17).

Similar arguments apply in the case $c_0 \neq 0$, except that now there are *two* ‘‘special directions’’, $|\psi_0\rangle$ and $|0\rangle$, to which $|\psi_t^\perp\rangle$ in (6) is always orthogonal.

From a different viewpoint, the situation may also be considered as a natural extension of previously established, non-dynamical “typicality” concepts [3, 17–19] into the dynamical realm: The vectors $\{|\psi_t^\perp\rangle\}_{t=0}^\infty$, explore a considerable part of the high dimensional orthogonal complement of $|\psi_0\rangle$ and $|0\rangle$, hence they are typically (for most t) almost orthogonal to a given vector (cf. (16)) and assume similar expectation values for a given observable (cf. (17)). For this reason, we henceforth denote the extension of (16) and (17) to arbitrary t as *typicality of the orthogonal dynamics* (TOD).

Exploiting TOD in (9) yields – after some straightforward but slightly tedious algebra – our final result

$$\mathcal{A}_t \simeq \bar{\mathcal{A}} + a f_t + a^* f_t^* + |f_t|^2 [\mathcal{A}_0 - \bar{\mathcal{A}} - a - a^*], \quad (18)$$

$$f_t := \frac{e^{-iE_0 t} g_t - p_0}{1 - p_0}, \quad g_t := \sum_{n=0}^N p_n e^{iE_n t}, \quad (19)$$

$$a := c_0 \langle \psi_0 | \mathcal{A} | 0 \rangle - p_0 \langle 0 | \mathcal{A} | 0 \rangle. \quad (20)$$

Specifically, if all level populations are small (see above) we thus obtain

$$\mathcal{A}_t \simeq \bar{\mathcal{A}} + |g_t|^2 [\mathcal{A}_0 - \bar{\mathcal{A}}]. \quad (21)$$

As a further corroboration of TOD, we have rederived the same result (18) by means of a more rigorous, but less enlightening and quite arduous generalization of the approach from [20–22]: The first step consist in skillfully “rearranging” the large number of energies $\{E_n\}_{n=1}^N$ in (1) and then to “redistribute” the corresponding level populations $\{p_n\}_{n=1}^N$, yielding a very accurate approximation in terms of an effective (auxiliary) model with nearly equally populated eigenstates [22]. In a second step, one can show that the so obtained effective relaxation dynamics is approximately invariant under the vast majority of all permutations of its auxiliary eigenstates, as worked out by way of generalizing [20, 21] in the PhD thesis [23]. Taking for granted that the “true” (non-permuted) model belongs to that vast majority, one eventually recovers (18).

Yet another confirmation of TOD can be obtained in the small t regime: Considering the set of all initial states $|\psi_0\rangle$ with the same values of c_0 and $\langle \psi_0 | \mathcal{A} | \psi_0 \rangle$ as the “true” $|\psi_0\rangle$, it can be shown along the lines of [24] that most of them satisfy (16) and (17) extremely well for $t \rightarrow 0$ under these sufficient (but not necessary) conditions: Among the levels $\{|n\rangle\}_{n=1}^N$, only those with energies E_n in some small (microcanonical) energy window are non-negligibly populated, and the concomitant diagonal and off-diagonal matrix elements $\langle m | \mathcal{A} | n \rangle$ satisfy the eigenstate thermalization hypothesis (ETH) [2, 25].

As a final validation of TOD, we will compare in the next Sec. IV our main prediction (18) with numerical results for a variety of specific examples. Before doing so, it is instructive to discuss the functions f_t and g_t from (19) in somewhat more detail:

First, we can conclude from (19) that $f_0 = 1$ and – similarly as in (12)–(15) – that $f_t \simeq 0$ for (most) sufficiently

large t . The intermediate t 's thus govern the non-trivial part of the temporal relaxation in (18).

Second, it is often useful to rewrite g_t from (19) by means of (1) as the survival amplitude of the initial state,

$$g_t = \langle \psi_t | \psi_0 \rangle. \quad (22)$$

Since $|\psi_t\rangle$ can be obtained by time-evolution methods [26, 27], diagonalizing the Hamiltonian is thus *not* mandatory to determine g_t .

Alternatively, (19) may also be written as

$$g_t = \int dE \rho(E) e^{iEt}, \quad \rho(E) := \sum_{n=0}^N p_n \delta(E_n - E), \quad (23)$$

i.e., $\rho(E)$ describes the system’s energy distribution and g_t is its Fourier transform. Note that the energy distribution is conserved under the dynamics, hence it can be inferred directly from the initial state. Moreover, for the small-to-moderate times t during which the nontrivial part of the relaxation takes place, it is not mandatory to know this distribution in all its details. Rather, already a reasonably good approximation of the main features of $\rho(E)$ will admit quite decent predictions for the Fourier transform g_t in (23), see also [20] for various specific examples along these lines.

IV. COMPARISON WITH NUMERICAL EXAMPLES

In the following subsections we compare our above obtained analytical predictions within numerical results. Moreover, we exemplify in Sec. IV C the extension of those predictions to situations where more than one level exhibits a non-small population.

A. XXZ model

Our first example is the integrable spin-1/2 XXZ-chain with anisotropy parameter Δ , magnetic field B , and periodic boundary conditions,

$$H = \sum_{i=1}^L S_i^x S_{i+1}^x + S_i^y S_{i+1}^y + \Delta S_i^z S_{i+1}^z - B S_i^z, \quad (24)$$

where $S_i^{x,y,z}$ are the spin operators at lattice site i .

Focusing on $B \gg 1 + \Delta$ and introducing the abbreviations $B' := B - \Delta/2$, $B'' := B - \Delta$, one finds $|0\rangle = |\uparrow \dots \uparrow\rangle$ (all spins “up”) as ground state with energy $E_0 = -B'L/2$, followed by a first “band” of excited states $|n\rangle = \sum_{k=1}^L e_{n,k} |s_k\rangle$ with energies $E_n = E_0 + \cos(2\pi n/L) + B''$, where $n = 1, \dots, L$, $e_m := e^{i2\pi m/L}/\sqrt{L}$, and where $|s_k\rangle$ represents the state with all but the k -th spin “up”. Thus, the “gap” between this energy band and E_0 equals $B'' - 1 \gg 1$ for even L , and is slightly

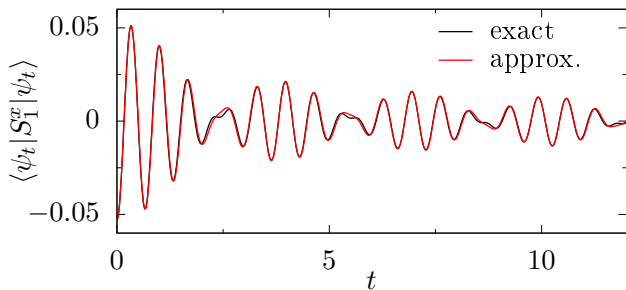


FIG. 1: Time-dependent expectation values of the observable $A = S_1^x$ according to the exact Eqs. (1), (9) and the approximation (18) for the XXZ chain from (24) with $L = 1000$, $B = 10$, and $\Delta = 0.5$. The initial state $|\psi_0\rangle$ was generated by a quantum quench as detailed in the main text, resulting in $p_0 \simeq 0.997$ and $p_{\max} \simeq 3.5 \cdot 10^{-6}$.

larger than $B'' - 1$ for odd L . After another gap of comparable size, there follows a second band, and so on.

As initial condition $|\psi_0\rangle$ we choose the ground state of the modified Hamiltonian

$$\tilde{H} := H + \Pi b_x S_1^x \Pi. \quad (25)$$

Here, $b_x S_1^x$ models an “impurity” in terms of a magnetic field b_x , which is perpendicular to the B field in (24), and which only acts on one site of the spin chain. Due to the periodic boundary conditions, we have chosen the first site without loss of generality. Furthermore, $\Pi := \sum_{n=0}^L |n\rangle\langle n|$ in (24) is the projector on the subspace spanned by the ground state and the first band of excited states of H , and therefore eliminates the effects of the second and higher bands. Focusing on $B'' \gg 1$ and not too large b_x , it is reasonable to expect, and can be confirmed by a more detailed calculation, that these omitted effects are indeed very weak. Altogether, our setup thus still amounts to a physically sensible quantum quench scenario (see introduction) with post-quench Hamiltonian (21), pre-quench Hamiltonian (25) and exhibiting one non-small level population.

Given this setup, a straightforward calculation then yields (without any further approximation) $|\psi_0\rangle = \nu \sum_{n=0}^L \gamma_n |n\rangle$, where $\nu := (\sum_{n=0}^L |\gamma_n|^2)^{-1/2}$, $\gamma_0 := 1$, $\gamma_{n \geq 1} := -\sqrt{\eta/L} e_n^* [E_n - E_0 + \eta q]^{-1}$, $\eta := (b_x/2)^2$, and where q is the smallest positive solution of the transcendental equation $Lq = \sum_{n=1}^L [E_n - E_0 + \eta q]^{-1}$. Solving this equation, and finally evaluating the exact expectation values according to Eqs. (1) and (9), and their approximative counterparts according to (18)-(20) is an easy numerical task up to rather large L values.

The so obtained results for the numerically exact expectation values of $A = S_1^x$ together with the corresponding analytical approximation from (18) are exemplified in Fig. 1 as black and red lines, respectively. The main observations are that the temporal decay exhibits a quite rich structure and that the analytics captures them remarkably well.

For the specific example in Fig. 1, we chose $b_x = 1$ in (24), and the numerically obtained quantitative values for the ground state population p_0 and for the second largest population p_{\max} from (15) are $p_0 \simeq 0.997$ and $p_{\max} \simeq 3.5 \cdot 10^{-6}$, respectively. Moreover, closer inspection of the numerical data (beyond the range displayed in Fig. 1) reveals that the oscillations of $\langle \psi_t | A | \psi_t \rangle$ decrease rather slowly. Quantitatively, the envelopes seem to asymptotically approach $\bar{A} = 0$ in Fig. 1 essentially as $t^{-1/2}$ for large times. We finally mention that further increasing L in Fig. 1 did not result in any notable changes of the two curves.

B. Modified XXZ model

As a second example, we omit the B -field in (24) and include next-nearest neighbor interactions, yielding

$$H = \sum_{i=1}^L S_i^x S_{i+1}^x + S_i^y S_{i+1}^y + \Delta S_i^z S_{i+1}^z + \Delta' S_i^z S_{i+2}^z \quad (26)$$

with periodic boundary conditions, and spin-1/2 operators $S_i^{x,y,z}$ acting on lattice site i .

This model is integrable for $\Delta' = 0$ and non-integrable otherwise. Given Δ' , the energy spectrum exhibits a gap for sufficiently large Δ (for instance $\Delta > 1$ when $\Delta' = 0$ [14]). More precisely, the two lowest energies are almost degenerate (approaching an exact degeneracy for $L \rightarrow \infty$), and are separated by a gap (which persists for $L \rightarrow \infty$) from all other energies [28]. For the large but finite L 's and small-to-moderate t 's of interest to us, the two almost degenerate lowest energies can be safely approximated as being strictly degenerate (a rigorous bound for the corrections is provided in Appendix B of [22]). As detailed below (1), the situation thus effectively amounts to a single (non-degenerate) ground state, separated by a gap from the excited states. As initial condition $|\psi_0\rangle$ we choose the Néel state $|\uparrow\downarrow\uparrow \dots \downarrow\rangle$ (tensor product of alternating single-spins “up” and “down”), and we tacitly focus on even L from now on. At the same time, this $|\psi_0\rangle$ is the ground state of (26) when $\Delta \rightarrow \infty$, i.e., our setup may again be viewed as a quantum quench scenario and exhibits a non-small population p_0 for sufficiently large post-quench values of Δ in (26) [14, 29–33].

Employing numerical exact diagonalization (ED) of the Hamiltonian (26) for moderate system sizes L , it is straightforward to simulate the time evolution of the initial state $|\psi_0\rangle$ (cf. Eq. (1)), and to compute the expectation values of the desired operators (cf. Eq. (9)). Moreover, since ED yields the ground state $|0\rangle$, as well as all p_n and E_n , also our theoretical prediction (18)-(20) can be readily evaluated. Both the numerical data and the analytical approximations for $L = 16$ in Figs. 2 and 3 have been obtained along these lines.

As usual, since the z -component of the total spin is conserved for all values of Δ and Δ' in (26), i.e.,

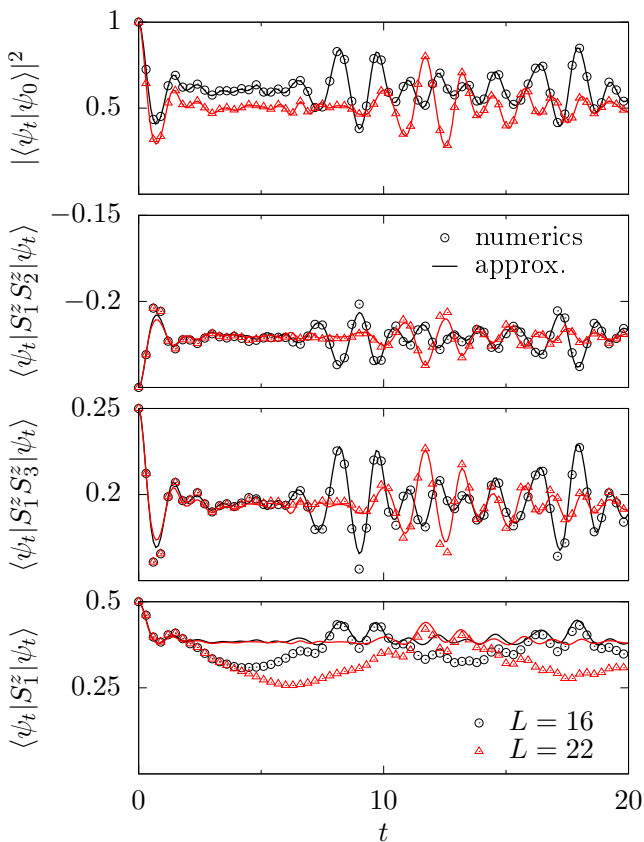


FIG. 2: Time-dependent expectation values of the observables $A = |\psi_0\rangle\langle\psi_0|$, $A = S_1^z S_2^z$, $A = S_1^z S_3^z$, and $A = S_1^z$ for the non-integrable spin-chain model from (26) with $\Delta = 3$, $\Delta' = -0.5$, $L = 16$ (black), $L = 22$ (red), and initial condition $|\psi_0\rangle = |\uparrow\downarrow\uparrow\dots\downarrow\rangle$ (Néel state). Symbols: Numerical results as detailed in the main text. Lines: Analytical approximation (18).

$[H, \sum_i S_i^z] = 0$, we can restrict ourselves to the diagonalization of the zero-magnetization subsector. Nevertheless, ED is practically feasible only up to relatively small (even) L values.

In order to also cover larger L values, we adopted an alternative numerical approach. The first key point is to utilize for the function g_t in (19) the alternative expression in terms of the survival amplitude from (22) (see also (29) below). Hence, full ED can be circumvented by solving the time-dependent Schrödinger equation iteratively, e.g., by means of a Runge-Kutta scheme with small time step [34], or also by other sophisticated approaches [35]. The quantities $|0\rangle$, c_0 , and p_0 in (19) and (20) can then be obtained by means of standard Krylov-subspace techniques. Both the numerical data and the analytical approximations for $L = 22$ in Fig. 2 and Fig. 3 have been obtained along these lines.

In Figs. 2 and 3 we compare the so obtained numerical results with the analytical prediction from (18) for the four observables $A = |\psi_0\rangle\langle\psi_0|$ (survival probability of the initial state), $A = S_1^z S_2^z$ (correlation of neighboring

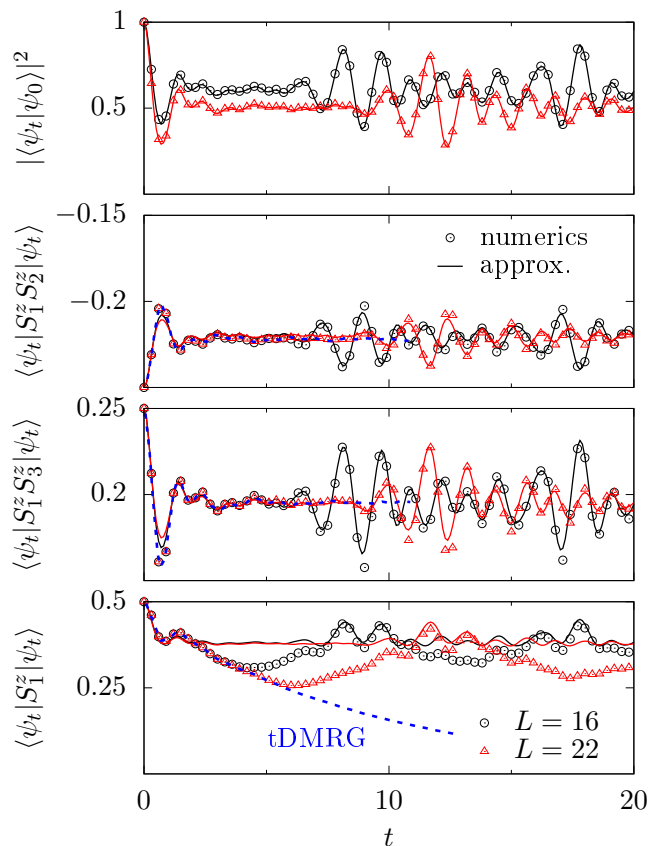


FIG. 3: Same as Fig. 2 but for an integrable model with $\Delta = 4$ and $\Delta' = 0$. Moreover, the time-dependent density matrix renormalization group (tDMRG) results from Refs. [29, 30] are indicated as dashed blue lines.

spins), $A = S_1^z S_3^z$ (next-nearest neighbor correlation), and $A = S_1^z$ (single spin). (Note that the specific lattice site is arbitrary due to the periodic boundary conditions in (26) and the initial Néel state.) Our first observation is that the non-integrable and integrable examples in Fig. 2 and Fig. 3 behave quite similarly. Second, the agreement between our numerical solutions (for $L = 16$ and $L = 22$) and the theoretical approximation is quite good, at least for the first three observables $A = |\psi_0\rangle\langle\psi_0|$, $A = S_1^z S_2^z$, and $A = S_1^z S_3^z$ (the fourth observable will be discussed in more detail later)

As opposed to Fig. 2, in the case depicted in Fig. 3 also time-dependent density matrix renormalization group (tDMRG) results are available from the literature [29, 30] and are shown as dashed blue lines. In contrast to our own numerics for $L = 16$ and $L = 22$, these tDMRG studies from [29, 30] were designed to approximate the thermodynamic limit $L \rightarrow \infty$.

In view of those results for $L \rightarrow \infty$, and since our main objective is to illustrate the validity of the theoretical prediction (18) for large but fixed values of L , we refrained from a more detailed finite-size scaling analysis.

In all depicted cases, we numerically found $p_0 \simeq 0.78$ for the ground state population and $p_{\max} \simeq 0.05$ for the

second largest population from (15). More precisely, both values decrease with increasing L but only extremely slowly. On the other hand, we recall that p_{\max} must be sufficiently small to guarantee equilibration (see introduction), and to satisfy our present condition (15). The fact that $p_{\max} \simeq 0.05$ is still not really small explains why the expectation values in Figs. 2 and 3 still do not equilibrate too well for large t , but rather keep “oscillating” quite notably about their long-time average. Moreover, this also seems to be a main reason for the remaining deviations of (18) from the numerics in Figs. 2 and 3. Unfortunately, substantially smaller p_{\max} values would require numerically unfeasibly large L 's. For the rest, we still find it remarkable that the prediction (18) often reproduces quite reasonably even those numerically obtained oscillations at large t . Apparently, the requirement of small p_{\max} values is quantitatively less stringent in (15) than with respect to equilibration.

In other words, the remnant “oscillations” for large t may be interpreted as finite L -effects, which, similarly as p_{\max} , decrease only very slowly with increasing L . Besides our numerics, also the tDMRG results are in agreement with (and thus provide further support to) this interpretation. More precisely speaking, our finite L results compare quite well with the tDMRG ($L \rightarrow \infty$) approximations for small-to-moderate t , but start to deviate for larger t values by developing the above mentioned “oscillations”. With increasing L , the onset of those deviations moves towards larger times. The latter effect is in fact considerably more pronounced than the simultaneous, but much weaker reduction of the oscillation amplitude with increasing L .

Turning to the last observable $A = S_1^z$ in Figs. 2 and 3, the agreement between our numerical solutions (for $L = 16$ and $L = 22$) and the theoretical approximation is still satisfying for small t and to some extent also for large t . In fact, the agreement with an appropriately generalized theory becomes again very good for even larger times, as we will see in the next subsection. On the other hand, for the intermediate times there remains a notable disagreement between theory and numerics, but also between our numerics and the tDMRG results. Apparently, we are dealing with some quite subtle and obstinate finite L effects for moderate-to-large t (see also Ref. [30]). More precisely speaking, the reason for those deviations seems to be that in this specific example the limits $t \rightarrow \infty$ and $L \rightarrow \infty$ apparently do not commute. Indeed, focusing first on the thermodynamic limit $L \rightarrow \infty$, it seems quite reasonable to expect, and is also supported by the tDMRG results in Fig. 3, that the expectation value $\langle \psi_t | S_1^z | \psi_t \rangle$ approaches zero for large times t . On the other hand, the numerical results for finite L in Fig. 3 substantially deviate from the latter relaxation behavior of the tDMRG data beyond some “critical” time, which increases with L . (In fact, this crossover seems to be closely connected with the onset of the above mentioned “oscillations”.) Therefore, it may not be so surprising that our simple theory misses those

quite subtle effects of the competition between the two non-commuting limits, especially in the transition region (moderate t in Figs. 2 and 3) between the regime where the large L limit “wins”, and the regime where the large t behavior at finite L takes over.

C. Two levels with non-small populations

We consider the same setup (and notation) as before, except that now *two* levels, namely those with indices $n = 0$ and $n = 1$, may exhibit non-small populations p_0 and p_1 . As explained below Eq. (1), we again can and will exclude degeneracies. In particular, we assume that $E_0 \neq E_1$.

In principle, the extension of the TOD concept from Sec. III is straightforward, however, carrying out the actual calculations is a quite arduous task (see also above Eq. (18)). Omitting them here, one finally obtains

$$\mathcal{A}_t \simeq \bar{A} + \kappa_t + \kappa_t^* + |\tilde{f}_t|^2 [\mathcal{A}_0 - \bar{A} - \kappa_0 - \kappa_0^*], \quad (27)$$

$$\tilde{f}_t := \frac{g_t - p_0 e^{iE_0 t} - p_1 e^{iE_1 t}}{1 - p_0 - p_1}, \quad (28)$$

$$g_t := \sum_{n=0}^N p_n e^{iE_n t} = \langle \psi_t | \psi_0 \rangle, \quad (29)$$

$$\kappa_t := \lambda_0 \chi_0(t) + \lambda_1 \chi_1(t) + \gamma e^{i(E_1 - E_0)t}, \quad (30)$$

$$\lambda_0 := c_0 \langle \psi(0) | A | 0 \rangle - p_0 \langle 0 | A | 0 \rangle - \gamma, \quad (31)$$

$$\lambda_1 := c_1 \langle \psi(0) | A | 1 \rangle - p_1 \langle 1 | A | 1 \rangle - \gamma^*, \quad (32)$$

$$\gamma := c_0 c_1^* \langle 1 | A | 0 \rangle, \quad (33)$$

$$\chi_\nu(t) := \tilde{f}_t e^{-iE_\nu t} \quad (\nu = 0, 1). \quad (34)$$

In analogy to Eq. (15), the main precondition for the above results now takes the form

$$\max_{n \geq 2} p_n \ll 1 \quad (35)$$

By means of a similar arguments as between Eq. (15) and Eq. (16), one can infer from (28) that $\tilde{f}_t \simeq 0$ for the vast majority of all sufficiently large t . The same property is inherited by $\chi_\nu(t)$ in (34), hence κ_t in (30) is dominated by the last term on the right hand side. Finally, (27) can then be approximated for most sufficiently large t as

$$\mathcal{A}_t \simeq \bar{A} + \gamma e^{i\omega t} + \gamma^* e^{-i\omega t} \quad (36)$$

$$\omega := (E_1 - E_0)/\hbar, \quad (37)$$

i.e., \mathcal{A}_t oscillates about the temporal mean value \bar{A} with frequency ω and amplitude $2|\gamma|$ (see also (33)).

The previously obtained results for a single level with non-small population p_0 are readily recovered by formally setting $p_1 = 0$ and thus $c_1 = 0$ (see also discussion below Eq. (17)).

As an example we consider again the model from (26) with a Néel state $|\uparrow\downarrow\uparrow\dots\downarrow\rangle$ as initial condition. Focusing

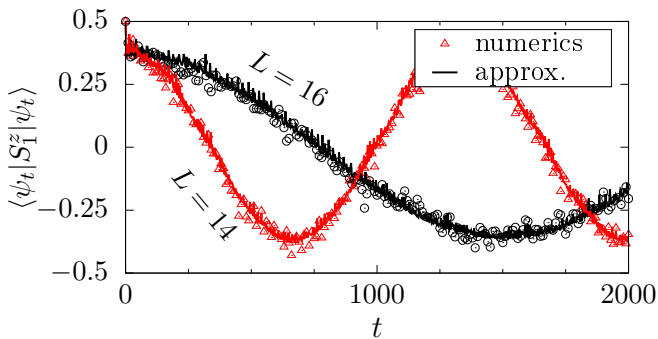


FIG. 4: Time-dependent expectation values of $A = S_1^z$ for $\Delta = 4, \Delta' = 0$ (analogous to bottom panel of Fig. 3, but now for times up to $t = 2000$), and for system sizes $L = 14$ and $L = 16$. The numerically observed slow oscillations of $\langle \psi_t | A | \psi_t \rangle$ (resulting from the level splitting between the two almost-degenerate eigenstates) are remarkably well captured by our generalized analytical approximation from (27)-(34).

again on the gapped regime, the two lowest energies of this model are for large L almost degenerate, approaching an exact degeneracy for $L \rightarrow \infty$, and are (almost) equally populated by the Néel state. For the reasonably large L 's and small-to-moderate t 's which we considered so far, those two almost degenerate lowest energies could thus always be safely approximated as being strictly degenerate. Indeed, our generalized theoretical prediction (27)-(34) would be practically indistinguishable from the solid lines in Figs. 2 and 3.

Therefore, we now turn to even much larger times t , for which the difference between the two lowest energies is no longer negligible, and hence the generalized theory (27)-(32) must be employed. In doing so, we adopted the same numerical ED methods as described in detail in the previous subsection.

Fig. 4 shows the so obtained time-dependent expectation values $\langle \psi_t | S_1^z | \psi_t \rangle$ for two different system sizes $L = 14$ and $L = 16$. In particular, the black line and symbols ($L = 16$) correspond to those in the bottom panel of Fig. 3, except that they now cover a much larger time interval up to $t = 2000$. Most notably, for such long times, we find that the observable $A = S_1^z$ gives rise to approximately harmonic oscillations, in good agreement with the theoretical asymptotics (36). In particular, the oscillations persist up to arbitrarily large times, i.e., we are dealing with an example which does not exhibit equilibration in the long-time limit.

As said above, the energy difference between the almost degenerate levels is known to decrease with increasing L . In agreement with (37), the oscillation frequency in Fig. 4 is indeed observed to decrease with increasing L .

Finally, and again in close analogy to the previous subsection, we numerically found that $p_0 \simeq p_1 \simeq 0.39$, $\max_{n \geq 2} p_n \simeq 0.05$ and that both values decrease very slowly with L . Accordingly, the amplitude of the oscillations in Fig. 4 decreases very little with increasing L .

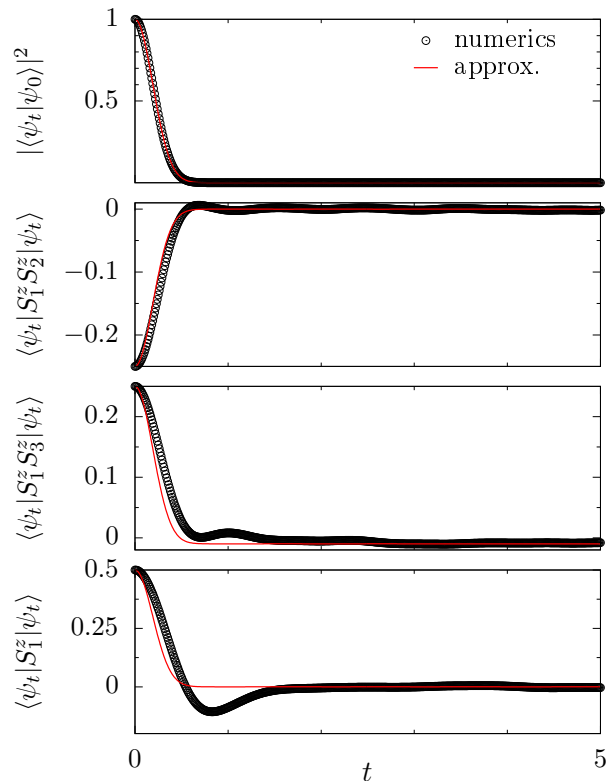


FIG. 5: Time-dependent expectation values of $A = |\psi_0\rangle\langle\psi_0|$, $A = S_1^x S_2^z$, $A = S_1^z S_3^z$, and $A = S_1^z$ for the fully-connected model (38) with $L = 16$ sites and a fixed choice of the random couplings $J_{ij}^{x,y,z}$. Symbols: Numerical results (ED). Lines: Analytical approximation (21).

D. Small populations of all levels

In this subsection, we further elaborate on the special case that *all* level populations p_n are small (see also below Eq. (17)), including a comparison of numerical results with the corresponding simplified analytical approximation from (21).

To this end, we consider the fully connected spin model

$$H = \sum_{i=1}^L \sum_{j>i}^L J_{ij}^x S_i^x S_j^x + J_{ij}^y S_i^y S_j^y + J_{ij}^z S_i^z S_j^z, \quad (38)$$

where the couplings $J_{ij}^{x,y,z}$ are independent, Gaussian distributed random variables with zero mean and unit variance, and we choose again a Néel state $|\uparrow\downarrow\uparrow\dots\downarrow\rangle$ as initial condition. Two important differences in comparison with the previous model (26) are: First, the random couplings eliminate any spatial structure and lift all symmetries of the model so that the initial Néel state is randomly spread over the whole energy basis with all p_n being very small quantities on the order of 2^{-L} . Second, the total magnetization is generally not any more conserved ($[\sum_i S_i^z, H] \neq 0$) so that the resulting dynamics has to be understood with respect to the full Hilbert space with

dimension 2^L . Apart from that, we employed the same numerical ED methods as before.

For this model and initial condition, we depict in Fig. 5 our numerical and analytical results for the usual four observables $A = |\psi_0\rangle\langle\psi_0|$, $A = S_1^z S_2^z$, $A = S_1^z S_3^z$, and $A = S_1^z$, where we have used one fixed realization of the random couplings $J_{ij}^{x,y,z}$ in (38). Moreover, since finite-size effects are expected to be relatively weak in such a random and fully-connected model, we restrict our analysis to a single system size $L = 16$. For all observables shown in Fig. 5, we find that $\langle\psi_t|A|\psi_t\rangle$ exhibits a fast decay on short times scales $t \lesssim 1$, before equilibrating to its long-time value $\bar{A} \approx 0$. Our analytical approximation explains the numerical findings in Fig. 5 comparably well as in the previous cases in Figs. 2 and 3.

The example from Fig. 5 thus illustrates that our theory also covers cases where all p_n are small, i.e., beyond the situations at the actual focus of our paper, where one energy level exhibits a non-small population. For a more detailed exploration of the conceptual premises of such a theoretical approach we also refer to [22]. In particular, it turns out that both the considered observable and the initial state must be “sufficiently far” from any conserved quantity, since any such too close constant of motion would give rise to a slower temporal relaxation than predicted by our present theory. In the same vein, the special “regularity” of the initial Néel state may well be the cause of the remaining deviations between numerics and theory in Fig. 5.

V. CONCLUSIONS

While thermal equilibrium properties of gapped systems at low energies or in the ground state have been previously explored in considerable detail, the focus of

our present work is on the temporal relaxation of a far from equilibrium initial state. We put forward a new kind of typicality principle, named typicality of the orthogonal dynamics (TOD), which governs the equilibration of isolated many-body quantum systems: The (normalized) component of the system state $|\psi_t\rangle$ orthogonal to the initial state $|\psi_0\rangle$, and possibly also to one non-negligibly populated energy level $|0\rangle$, typically exhibits similar properties at early and at later times. As a consequence of TOD we obtained an analytical prediction for the temporal relaxation behavior, comparing very favorably with a variety of numerical test cases. Particular emphasis was laid on the previously hardly explored relaxation of systems with a non-small ground state population due to a gap in the energy spectrum. However, our prediction also covers considerably more general situations. In particular, the system may or may not be integrable and thus may or may not exhibit thermalization. In either case, a key role is played by the overlaps in (22) and/or the energy distribution in (23). Finally, we exemplified in Sec. IV C that our present approach can also be extended to situations where several energy levels exhibit non-small populations and hence the system is not even expected to equilibrate.

Acknowledgments

We are indebted to Masud Haque for additional explanations and numerical results concerning Ref. [14], Jürgen Schnack for bringing Ref. [15] to our attention, and Thomas Dahm for illuminating discussions. This work was supported by the Deutsche Forschungsgemeinschaft (DFG) within the Research Unit FOR 2692 under Grants No. 397303734, 397067869, and 355031190.

-
- [1] C. Gogolin and J. Eisert, Equilibration, thermalization, and the emergence of statistical mechanics in closed quantum systems, Rep. Prog. Phys. **79**, 056001 (2016).
 - [2] L. D’Alessio, Y. Kafri, A. Polkovnikov, and M. Rigol, From Quantum Chaos and Eigenstate Thermalization to Statistical Mechanics and Thermodynamics, Adv. Phys. **65**, 239 (2016).
 - [3] H. Tasaki, Typicality of Thermal Equilibrium and Thermalization in Isolated Macroscopic Quantum Systems, J. Stat. Phys. **163**, 937 (2016).
 - [4] F. Borgonovi, F. M. Izrailev, L. F. Santos, and V. G. Zelevinsky, Quantum chaos and thermalization in isolated systems of interacting particles, Phys. Rep. **626**, 1 (2016).
 - [5] T. Langen, T. Gasenzer, and J. Schmiedmayer, Prethermalization and universal dynamics in near-integrable quantum systems, J. Stat. Mech. 064009 (2016).
 - [6] T. Mori, T. N. Ikeda, E. Kaminishi, and M. Ueda, Thermalization and prethermalization in isolated quantum systems: a theoretical overview, J. Phys. B **51**, 112001 (2018).
 - [7] A. Hobson, *Concepts in Statistical Mechanics* (Gordon and Breach, New York, 1971).
 - [8] P. Reimann, Foundation of statistical mechanics under experimentally realistic conditions, Phys. Rev. Lett. **101**, 190403 (2008).
 - [9] N. Linden, S. Popescu, A. J. Short, and A. Winter, Quantum mechanical evolution towards equilibrium. Phys. Rev. E **79**, 061103 (2009).
 - [10] A. J. Short, Equilibration of quantum systems and subsystems, New J. Phys. **13**, 053009 (2011).
 - [11] A. J. Short and T. C. Farrelly, Quantum equilibration in finite time, New J. Phys. **14**, 013063 (2012).
 - [12] P. Reimann and M. Kastner, Equilibration of macroscopic quantum systems, New J. Phys. **14**, 043020 (2012).
 - [13] B. N. Balz and P. Reimann, Equilibration of isolated many-body quantum systems with respect to general distinguishability measures, Phys. Rev. E **93**, 062107 (2016).
 - [14] P. P. Mazza, J.-M. Stéphan, E. Canovi, V. Alba, M.

- Brockmann, and M. Haque, Overlap distributions for quantum quenches in the anisotropic Heisenberg chain, *J. Stat. Mech.* P013104 (2016).
- [15] V. Ya. Krivnov, D. V. Dmitriev, S. Nishimoto, S.-L. Drechsler, and J. Richter, Delta chain with ferromagnetic and antiferromagnetic interactions at the critical point, *Phys. Rev. B* **90**, 014441 (2014).
- [16] There may be isolated t 's with $\beta'_t = 0$ (for instance $t = 0$), for which $|\psi_t^\pm\rangle$ is defined via continuation.
- [17] S. Lloyd, Pure state quantum statistical mechanics and black holes, Ph.D. Thesis, The Rockefeller University, 1988, Chapter 3, arXiv:1307.0378.
- [18] S. Goldstein, J. L. Lebowitz, R. Tumulka, and N. Zanghì, Canonical typicality, *Phys. Rev. Lett.* **96**, 050403 (2006).
- [19] S. Popescu, A. J. Short, and A. Winter, Entanglement and the foundations of statistical mechanics, *Nat. Phys.* **2**, 754 (2006).
- [20] P. Reimann, Typical fast thermalization processes in closed many-body systems, *Nat. Commun.* **7**, 10821 (2016).
- [21] B. N. Balz and P. Reimann, Typical relaxation of isolated many-body systems which do not thermalize, *Phys. Rev. Lett.* **118**, 190601 (2017).
- [22] P. Reimann, Transportless equilibration in isolated many-body quantum systems, *New J. Phys.* **21**, 053014 (2019).
- [23] B. N. Balz, Dynamik von Quanten-Vielteilchensystemen; Equilibration, Thermalisierung und Typikalität in quanten-statistischer Mechanik, Ph.D Thesis, Universität Bielefeld 2018, pub.uni-bielefeld.de/record/2930989.
- [24] C. Bartsch and J. Gemmer, Dynamical Typicality of Quantum Expectation Values, *Phys. Rev. Lett.* **102**, 110403 (2009).
- [25] M. Srednicki, Thermal fluctuations in quantized chaotic systems, *J. Phys. A* **29**, L75 (1996).
- [26] S. Paeckel, T. Köhler, A. Swoboda, S. R. Manmana, U. Schollwöck, and C. Hubig, Time-evolution methods for matrix-product states, *Ann. Phys.* **411**, 167998 (2019).
- [27] A. Weiße, G. Wellein, A. Alvermann, and H. Fehske, The kernel polynomial method, *Rev. Mod. Phys.* **78**, 275 (2006).
- [28] H.-J. Mikeska and A. K. Kolezhuk, One-dimensional magnetism, in: *Quantum Magnetism* (Springer, Berlin, Heidelberg, 2004).
- [29] M. Fagotti, M. Collura, F. H. L. Essler, and P. Calabrese, Relaxation after quantum quenches in the spin- $\frac{1}{2}$ Heisenberg XXZ chain, *Phys. Rev. B* **89**, 125101 (2014).
- [30] P. Barmettler, M. Punk, V. Gritsev, E. Demler, and E. Altman, Quantum quenches in the anisotropic spin-1/2 Heisenberg chain: different approaches to many-body dynamics far from equilibrium, *New. J. Phys.* **12**, 055017 (2010).
- [31] L. Piroli, E. Vernier, P. Calabrese, and M. Rigol, Correlations and diagonal entropy after quantum quenches in XXZ chains, *Phys. Rev. B* **95**, 054308 (2017).
- [32] B. Pozsgay, M. Mestyán, M. A. Werner, M. Kormos, G. Zaránd, and G. Takács, Correlations after Quantum Quenches in the XXZ Spin Chain: Failure of the Generalized Gibbs Ensemble, *Phys. Rev. Lett.* **113**, 117203 (2014).
- [33] B. Wouters, J. De Nardis, M. Brockmann, D. Fioretto, M. Rigol, and J.-S. Caux, Quenching the Anisotropic Heisenberg Chain: Exact Solution and Generalized Gibbs Ensemble Predictions, *Phys. Rev. Lett.* **113**, 117202 (2014).
- [34] R. Steinigeweg, J. Gemmer, and W. Brenig, Spin and energy currents in integrable and nonintegrable spin- $\frac{1}{2}$ chains: A typicality approach to real-time autocorrelations, *Phys. Rev. B* **91**, 104404 (2015).
- [35] A. Weiße, G. Wellein, A. Alvermann, and H. Fehske, The kernel polynomial method, *Rev. Mod. Phys.* **78**, 275 (2006).